Thermal Chemistry of Trimethyl Acetic Acid on TiO_2(110)

J. M. White,*,†,‡ Janos Szanyi, and Michael A. Henderson*

Interfacial Chemistry and Engineering Group, Pacific Northwest National Laboratory, Richland, Washington 99352

Received: September 11, 2003; In Final Form: January 13, 2004

On the basis of temperature-programmed desorption and isothermal reaction mass spectrometry, the thermal surface chemistry of trimethyl acetic acid, $(CH_3)_3CCOOH$, dosed onto a well-characterized single-crystal TiO_2(110) surface is described. Deprotonation occurs at or below 300 K to form trimethyl acetate, $(CH_3)_3CCOO^-$, and hydroxide, OH^-. $(CH_3)_3CCOO^-$ is bound to exposed Ti^{4+} cations, and OH^- involves a bridging oxygen atom of the substrate. On the basis of temperature-programmed desorption and isothermal reaction mass spectrometry, the desorbing products include $(CH_3)_3CCOOH$, isobutene (i-C_4H_8), carbon monoxide, and water accompanied by smaller amounts of other products including methyl isopropenyl ketone ($CH_2{=}C(CH_3)C({=}O)CH_3$), isobutane ($i$-$C_4H_{10}$), and di-*tert*-butyl ketone, $(CH_3)_3CC({=}O)C(CH_3)_3$. Much of the $(CH_3)_3CCOO^-$ is relatively stable and decomposes to release mainly carbon monoxide and isobutene above 550 K with a maximum rate at 660 K. Thermal desorption to 750 K leaves a carbon-free surface that is indistinguishable from the initially clean surface. During dosing at 550 K, a steady-state reaction condition is realized with about half the adsorption sites being occupied at any instant.

I. Introduction

The surfaces and interfaces between different phases and materials often impact, even control, the properties of the resulting multicomponent systems. For example, the critical activity and selectivity properties of gas−solid or liquid−solid heterogeneous catalyst systems, thermal and photo, are determined by the structural and dynamical properties of surfaces that lie at the boundary separating the gas or liquid from the solid. In the environmental and health sciences, multicomponent arrays that integrate solid-state microelectronic devices with molecularly specific sensing elements are sought and typically involve interfaces between inorganic and organic materials. For these and other examples, the chemistry occurring between inorganic solids, such as oxides, and organic species is often a central issue. These practical considerations, in turn, invigorate widespread interest in measuring, understanding, and manipulating the atomic and molecular level characteristics of interfaces that link organic and inorganic components.

Using the tools of UHV surface science and focusing on saturation single layer adsorbate coverages, this paper describes the chemistry occurring at a well characterized inorganic single-crystal metal oxide surface, TiO_2(110), that is dosed with an organic compound, trimethylacetic acid, $(CH_3)_3CCOOH$ (TMAA). Single-crystal titanium dioxide continues to serve as a model for investigating transition metal oxide surface chemistries, including those involved in thermal catalysis, photocatalysis, and photoelectrochemistry.[1] The thermodynamically stable (110) face of rutile TiO_2 is widely studied and understood at a level approaching that of single-crystal metal and elemental semiconductor surfaces. Dosing TiO_2(110) at 300 K with an organic acid, RCOOH, typically results in acid−base surface chemistry; the acidic protons attach to surface oxygen anions, forming OH^-, and the accompanying basic carboxylate anions, $RCOO^-$, attach in ordered (2×1) fashion to Ti^{4+} cations of the rutile.[2,3] This paper focuses on the thermal chemistry of TMAA and its carboxylate, trimethyl acetate, $(CH_3)_3CCOO^-$, (TMA). Upon thermal activation, multiple decomposition paths are followed by the TMA and associated hydroxide. These lead to different gas-phase products—TMAA, isobutene, water, carbon monoxide, isobutane, methyl isopropenyl ketone, di-*tert*-butyl ketone and, importantly, leave a carbon-free surface upon heating to 750 K. In other work, we report on the photochemistry of TMA-covered TiO_2(110).[4] In related work,[5] we have shown that wetting TiO_2(110) with H_2O occurs in the absence of measurable oxygen atom vacancy and/or surface hydroxyl concentrations. On the other hand, TiO_2(110) covered with TMA is very hydrophobic, but becomes hydrophilic (wets) after TMA is photochemically removed.[5]

II. Experimental Section

Experiments were done in two standard ultrahigh vacuum chambers (base pressure of 2×10^{-10} Torr). One was equipped for temperature-programmed desorption (TPD), Auger electron spectroscopy (AES), high-resolution electron energy loss spectroscopy (HREELS), rear-view low-energy electron diffraction (LEED), secondary ion mass spectrometry (SIMS), and oxygen plasma treatment. The second chamber was equipped for X-ray photoelectron spectroscopy (XPS) using a Mg Kα anode and a hemispherical electron energy analyzer.

The TiO_2(110) substrate was cleaned routinely by sputtering/annealing (850 K) cycles to rid the surface of typical contaminants. Subsequently, the surface was either dosed with O_2 at 220 K to generate an oxidized surface or annealed in a vacuum at 850 K to generate a reduced surface. The *annealed* surface possessed surface bridging oxygen atom vacancies evidenced by dissociating water and leading to a recombination water desorption peak in TPD with intensity that was 6.5 ± 1% of

* Corresponding authors. E-mail: jmwhite@mail.utexas.edu (White), ma.henderson@pnl.gov (Henderson).

† Visiting professor and corresponding author.

‡ Permanent address: Department of Chemistry and Biochemistry, University of Texas, Austin, TX 78712.

10.1021/jp036713w CCC: $27.50
Published on Web 02/24/2004

undissociated H_2O monolayer coverage.[5,6] An excellent quality (1 × 1) LEED pattern was found for this surface. A perfect TiO_2(110) surface has an areal density of 5.2×10^{14} cm^{-2} exposed cations (Ti^{4+}) and anions (O^{2-}). For our conditions there were, in addition, 3.4×10^{13} bridging oxygen atom vacancies cm^{-2}.

Trimethylacetic acid, also known as pivalic acid, is a relatively small (102 amu) organic acid with 3 methyl groups and one tertiary carbon. It is dosable as vapor into ultrahigh vacuum; we measured a vapor pressure of 0.47 Torr at 300 K. TMAA vapor was dosed through a pinhole tubular doser arranged to direct the incident vapor onto the sample while avoiding the surrounding support structure and other nonsample surfaces. The relative dose was calculated as ($p \times t$) where p is the pressure drop across the pinhole (typically, between 0.06 and 0.47 Torr) and t is the dose time in seconds. After dosing and before initiating TPD into the apertured quadrupole mass spectrometer, the substrate was cooled to 100 K and rotated from the dosing position to align its surface normal with the cylinder axis of the quadrupole mass spectrometer.

Taking mass spectra while dosing TMAA proved informative. In these measurements, the sample was rotated 45° away from its normal TPD position to face the doser and was held at a selected temperature. While taking mass spectra, the doser was turned on, and then off, for selected times. To compare amounts of desorbing species in these isothermal experiments with amounts desorbing in TPD, the different detection geometry was accounted for by comparing TPD spectra taken in the two geometries. To account for background pressure rises during these dosing experiments, mass spectra were taken while dosing an inert stainless steel flag placed between the substrate and the doser. The profiles were subtracted from those gathered while dosing the substrate, and the difference was attributed to adsorption and reaction at the substrate.

To quantify the relative amounts of desorbing products, peak areas were determined by integration of intensity at mass m, I_m, vs t plots, where t is the time in seconds. Prior to integration, contributions from background and fragmentation of other species were subtracted. Monitoring TMAA, i-C_4H_8, i-C_4H_{10}, and CO was based on measured fragmentation patterns obtained by dosing these four molecules. For other species, we relied on published fragmentation patterns.[7] Constant low-level backgrounds were adequate, except for 18, 28, and 44 amu where sloping, often rather intense, backgrounds were required making integrated intensities subject to considerable uncertainty. To convert the integrated areas associated with the products to absolute coverages (species cm^{-2}), we directly dosed adsorbates so that, in subsequent TPD, the monolayer peaks were saturated. The integrated intensity vs time curves provide calibrated monolayer peak areas and, making use of either literature measurements of absolute saturation coverage or liquid-phase densities, these peak areas were used to convert monolayer intensities to molecules cm^{-2}. The numerical details are presented below.

For XPS, we dosed TMAA to saturation at 300 K on a clean surface, ramped the temperature (2 K s^{-1}) to a predetermined value, immediately recooled to 300 K, and gathered data for carbon, oxygen, and titanium. This cycle was repeated for numerous temperatures between 300 and 750 K and, from integrated intensities and line shapes, provides insight regarding species present on the surface as a function of temperature.

III. Results

Thermal Desorption. Thermal desorption spectra were obtained after dosing TMAA at three temperatures—100, 300, and 550 K—and cooling to 100 K. At 300 and 550 K, where multilayers do not form, we measured TPD only for saturation doses of TMAA. The latter temperature was chosen to simplify the overall profiles and to determine absolute coverages obtainable at these temperatures. The former temperature was chosen to provide for comparison with results for the 100 and 550 K results and, more importantly, to complement STM and photochemistry results reported elsewhere.[4,8] Regardless of the dosing temperature, TPD to 750 K led to a carbon-free surface as judged by AES and, for a 300 K dose, as judged by XPS.

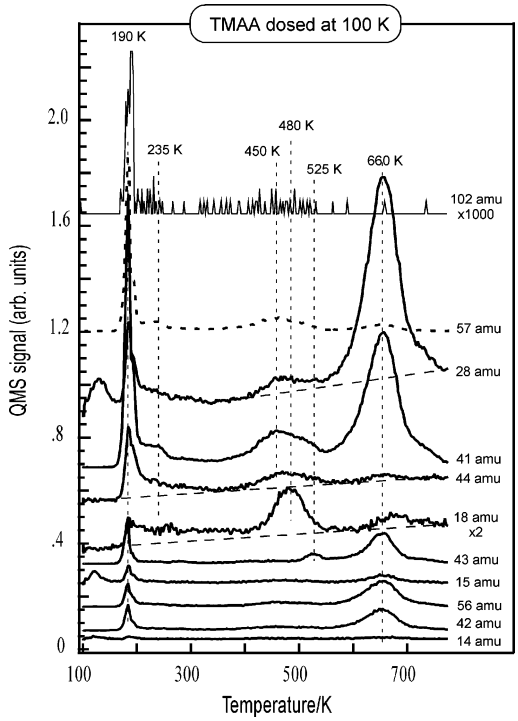

Figure 1. Temperature-programmed (2 K s^{-1}) desorption spectra for the indicated ions after a multilayer dose of TMAA on clean and vacuum annealed TiO_2(110) held at 100 K.

TPD profiles taken after a multilayer dose at 100 K (Figure 1) have peaks at 190, 235, 450−480, 525, and 660 K. Most of the profiles are particularly intense at 190 and 660 K. The baselines rise very little during the temperature ramp except for the 18, 28, and 44 amu profiles. The rising baselines (dashed lines) associated with these three profiles are attributed to desorption from nonsample surfaces. In analyzing TPD data quantitatively, linear backgrounds were subtracted from all the profiles to give zero intensity at 170 and 750 K.

The parent ion of TMAA (102 amu), although very weak, is clearly evident at 190 K and, arguably, contributes signal equal to the noise level from 200 to 240 and 400 to 550 K. Above 550 K, there is no evidence for any 102 amu intensity. For all the other profiles, the peaks at 190 K, the shoulders at 200 K, and the peaks at 235 K are attributable to TMAA desorption. The 43, 56, and 57 amu profiles turn out to be particularly relevant in our analysis. When scaled to each other at 190 K, these all track between 170 and 440 K indicating that, for doses at 100 K, these four profiles are fully accounted for by TMAA. Detailed analysis indicates that the only other species desorbing up to 440 K is H_2O, monitored by the 18 amu profile. This signal is of central interest but difficult to analyze quantitatively because of variable background and pumping speed contributions. The 18 amu peaks at 190 and 235 K are attributed to fragmentation of TMMA. Below 440 K, this leaves an H_2O desorption peak at 270 K and a rapidly rising H_2O signal above

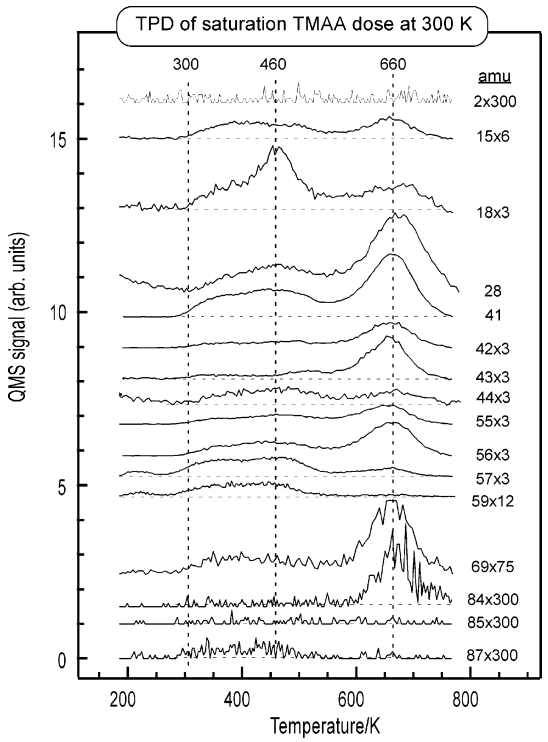

Figure 2. Temperature-programmed (2 K s^{-1}) desorption spectra for the indicated ions after a saturation dose of TMAA on clean and vacuum-annealed TiO_2(110) held at 300 K.

400 K that maximizes well above 440 K. Strikingly, there is also an H_2O peak at 680 K, the highest temperature peak found among all the products.

Since TPD after doses at 100 K are readily described, below 300 K, in terms of desorption dominated by TMMA and H_2O, we turn to the much more complex region above 300 K and compare TPD after doses at 100 and 300 K. In one set of eleven experiments, TPD profiles of selected ions between 14 and 90 amu were measured after a saturation dose at 300 K followed by cooling to below 200 K. Each experiment monitored 10 ions, three of which were common (43, 56, and 57 amu) and found to have peak areas (determined from intensity vs time curves) that were reproducible to within 5%. The 2 amu signal was monitored in a separate experiment. The background-subtracted TPD profiles of selected ions (Figure 2), like those of Figure 1, have intense maxima in the region above 550 K but differ from Figure 1 between 300 and 600 K. For example, the 57 amu profiles have maxima with nearly the same absolute intensity, but the distributions differ and the total area is 50% higher for the 300 K dose (Figure 3). The trailing edges of the peaks at 450 and 660 K are in good agreement, but there is significant broadening of both toward lower temperatures for the 300 K dose. Furthermore, the intensity between 300 and 550 K appears to involve at least two local maxima. Very similar differences are evident in the 56 amu signals (see below). The case for 43 amu is somewhat different. Relative to the 100 K dose, a 300 K dose exhibits intensity between 300 and 450 K that remains relatively weak, the peak at 525 K is suppressed while the peak at 660 K is broadened only slightly and has the same intensity to within 10%.

With this in mind, we examine the intense 660 K desorption peaks. On the basis of a thorough analysis of these profiles, comparing them with measured and published fragmentation patterns,[7] we conclude that desorption in this region is dominated by *i*-C_4H_8 and CO with smaller contributions from H_2O, methyl isopropenyl ketone (MIK, $CH_2{=}C(CH_3)C(=O)CH_3$), *i*-C_4H_{10},

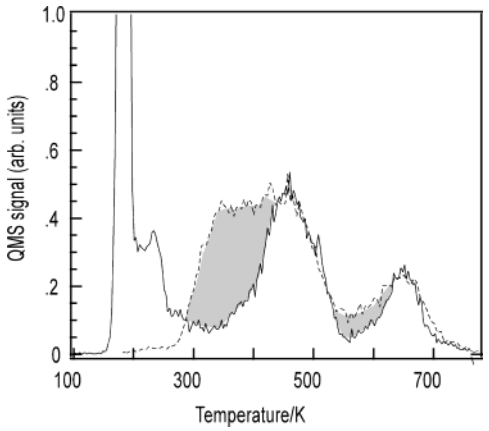

Figure 3. Comparing 57 amu profiles for TMAA doses at 100 and 300 K.

and either or both TMAA and di-*tert*-butyl ketone (di-*t*-BK, $(CH_3)_3CC(=O)C(CH_3)_3$). Support for *i*-C_4H_8 is based on the relatively strong signals at 56 and 55 amu, accompanied by weaker signals (not shown) in the 49 to 54 amu region that closely match the measured fragmentation pattern for this molecule. Further, *i*-C_4H_8 contributes a significant fraction to the exceptionally strong 41 and 28 amu signals at 660 K. Most of the remaining 28 amu signal is accounted for by CO desorption.

Since *i*-C_4H_8 has negligible intensity at 57 amu ($C_4H_9^+$) other species must contribute. While 57 amu is an intense TMAA fragment, the following analysis shows that other species must make a significant contribution above 550 K. Because they are more distinctive, the fragments at 102, 87, and 59 amu are helpful in tracking TMAA desorption even though they are ~1000×, ~100×, and ~10× weaker, respectively, than 57 amu. Above 550 K, the 102, 87, and 59 amu profiles are not strong enough to account for all the 57 amu signal as TMAA. The coupling of two TMA moieties would give di-*tert*-butyl ketone (di-*t*-BK, $(CH_3)_3CC(=O)C(CH_3)_3$), the mass spectrum of which has a very intense 57 amu fragment and a much weaker 85 amu fragment.[7] While there is no detectable signal above background at 85 amu (Figure 2), we expect the 57 amu signal to be 50 to 100x larger. Thus, some di-*t*-BK is plausible. In the assessment described below of amounts desorbed above 550 K, we are not able to separate the contributions of TMAA and di-*t*-BK. The calculation is based on 57 amu being dominated by TMAA.

The 84 amu signal (Figure 2) shows intensity only above 550 K and, thus, indicates a product that is not a major contributor at lower temperatures. It is attributed to methyl isopropenyl ketone (MIK, $CH_2{=}C(CH_3)C(=O)CH_3$) the published fragmentation pattern of which includes strong contributions to 41, 43, and 69 amu, but a negligible contribution at 57 amu.[7] Forming this species requires concerted deprotonation and methyl migration within a single TMA. The relatively strong 69 amu signal at 660 K is consistent with a contribution from MIK.

Scaling the 84 and 43 peaks at 660 K gives good overlap above but not below 600 K, i.e., there is excess 43 amu signal between 450 and 600 K. Isobutane fragmentation is dominated by 43 amu and can account for the excess. It is clearly formed during photolysis.[9] Another possibility is 3-methyl 2-butanone, (MB, $(CH_3)_2CHC(=O)CH_3$), that, besides a peak at the parent mass of 86 amu, shows weak intensity at 71 amu and strong signals at 41 and 43 amu, all consistent with our observations. In the analysis below, coverage estimates assume that the 43

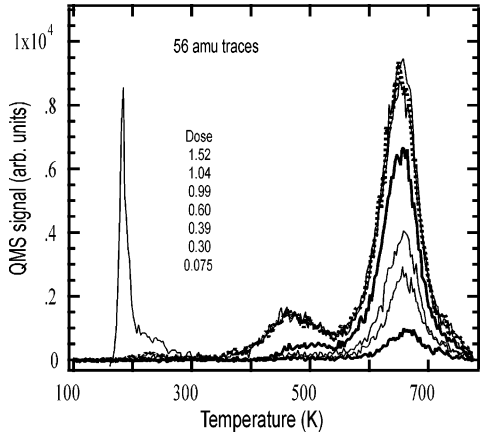

Figure 4. Variation of the 56 amu ion intensity in TPD (2 K s^{-1}) after the indicated doses of TMAA at 100 K. The intensities above 300 K saturate and the dosing scale is arbitrarily set to unity ($D = 1$) for the smallest dose at 100 K for which the intensity above 300 K saturates. The seven doses utilized are indicated and, from lowest to highest, correspond to curves from bottom to top in the 660 K region. Above 300 K, the 56 amu signal is, with some adjustment for contributions from TMAA fragmentation, diagnostic for isobutene desorption.

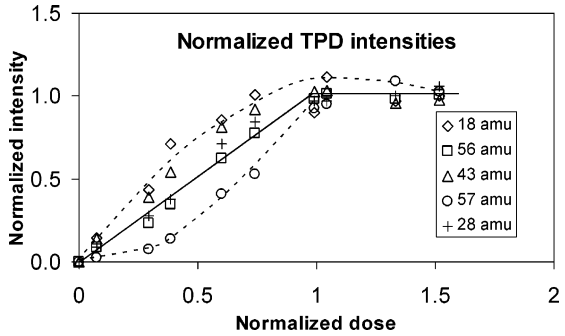

Figure 5. Using the dosing scale described in the text and the caption of Figure 4, this graph summarizes the integrated intensity of the indicated TPD ion traces as the dose, *D*, varies from zero to 1.5. The intensity for each ion is normalized to unity at $D = 1.5$.

signal can be approximated using measured data for *i*-C_4H_{10}. Other unassigned species taken together contribute no more than 5% to the total; for example, there is weak intensity at 69 amu that extends downward to 300 K and cannot be accounted for as MIK, *i*-C_4H_{10}, or TMAA.

Analysis of other profiles reveals no other products. For example, the 15 and 16 amu profiles are accounted for by fragmentation of higher mass precursors. Similarly, peaks in the 44 amu profile for are accounted for by species other than CO_2. We find no evidence for desorption of any species containing only 2 or 3 carbon atoms, i.e., no C_2 or C_3 hydrocarbons or partially oxidized hydrocarbons. Finally, the 2 amu signal shows no intensity above background.

Since the 56 amu profiles are dominated by *i*-C_4H_8, a dominant product, its development for varying doses, *D*, at 100 K, is of interest (Figure 4). For the lowest dose (0.075 units), there is a single peak at 660 K. As the dose increases, this peak grows and a second peak emerges near 500 K. The intensity profile in this region shifts toward lower temperatures with increasing dose. For doses (1.04 and 1.52 units) exceeding a critical value (arbitrarily defined as $D = 1$), the intensity above 300 K saturates and only the 190 K peak and its shoulder grow. For doses less than this critical value, the 56 amu integrated intensity between 300 and 750 K increases linearly (Figure 5).

In the region where the 56 amu intensity is saturated, other intensities also saturate, e.g., 18, 28, 43, and 57 amu (Figure 5). For $D < 1$, the 28 amu intensity follows the same linear pattern as 56 amu but the others do not. The relative 57 amu intensity grows much more slowly for the lowest doses and then rises nonlinearly; 18 amu rises nonlinearly and more rapidly than 56 amu; and 43 amu rises linearly but more rapidly than 56 amu for low doses.

TABLE 1: Desorbed Amounts for TMAA Doses at 100 K That Saturate TPD States above 300 K

molecule	from TMAA decomposition saturation TPD/ 10^{14} cm^{-2}	reference ML coverage/ 10^{14} cm^{-2}
CO	0.60	5.2
isobutane + MIK	0.12	3.7
isobutene + di-*tert*-butyl ketone	0.42	2.6
TMAA	0.61	2.6[a]
water	0.48	5.2

[a] From the intensity in "1 ML" of TMAA desorbing in the TMAA multilayer peak.

Even without accounting for fragmentation patterns, the following picture emerges. The 56 amu signal is dominated by isobutene, 43 by isobutane and methyl isopropenyl ketone, 28 by carbon monoxide, 18 by water, and 57 by TMAA. To approach a quantitative assessment, we made use of measured fragmentation patterns and monolayer doses of TMAA, *i*-C_4H_8, *i*-C_4H_{10}, and CO and, since we did not directly dose it, estimated contributions from MIK at high temperatures. For our system, the contribution of TMAA to I_{43} is $0.26 \times I_{57}$ and to I_{56} is $0.10 \times I_{57}$. The CO desorption was determined using the relation (I_{28}- $2.1 \times I_{56} - 0.17 \times I_{43} - 0.51 \times I_{57}$) to account for significant 28 amu contributions due to fragmentation of other species. When searching for CO_2 desorption, (I_{44}- $0.4 \times I_{57} - 0.06 \times I_{43}$) was used to account for fragmentation of TMAA, MIK, and *i*-C_4H_{10} at 44 amu.

As a measure of internal consistency, the I_{41} profile proved valuable because the fragmentation patterns of TMAA, isobutene, MIK, and isobutane as well as several other plausible products, have large 41 amu signals. Thus, a predicted I_{41} profile can be constructed ($I_{41,pred} = 0.68 \times I_{43} + 4.0 \times I_{56} + 0.9 \times I_{57}$) based on the contributions from TMAA, *i*-C_4H_8, and *i*-C_4H_{10}, and compared to the measured I_{41} profile. This ignores contributions from MIK but since its fragmentation pattern gives about equal intensities of I_{41} and I_{43}, the above function will account for most of its contribution provided it does not dominate. The difference spectra (not shown) lie well within the experimental uncertainty of the measured fragmentation patterns and intensity profiles. We take this information as confirmation that desorption does not include contributions of more than a few percent from any species with 3 or more carbon atoms other than TMAA, isobutene, MIK, and isobutane.

From the average of four doses in the saturation region, and after accounting for fragmentation as described in the Experimental Section, we estimated (Table 1) absolute amounts desorbing per unit area. These amounts are based on absolute monolayer coverages (last column of Table 1) and measured TPD intensities (I_m vs *t*) for directly dosed monolayers. In this analysis, we are unable to separate the contributions of *i*-C_4H_{10} and MIK. The absolute monolayer coverages of CO and H_2O were assigned on the basis of literature reports that the ratio of chemisorbed species to exposed Ti^{4+} is unity for both.[6,10] For TMAA + di-*tert*-butyl ketone, isobutene, and the combination of isobutane and MIK, the values were assigned after considering the size of each molecule and plausible chemisorption

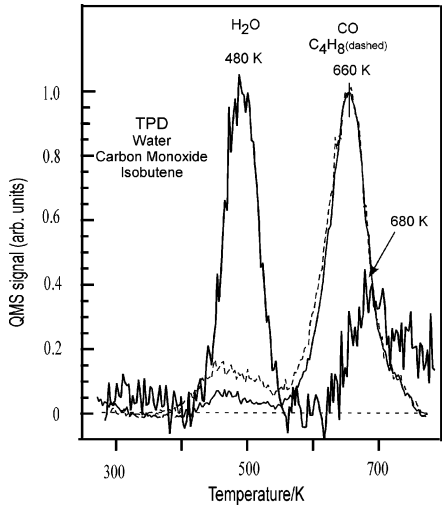

Figure 6. For $D > 1$, the H_2O, CO, and i-C_4H_8 TPD intensity profiles scaled to unity at their global maxima. The CO and i-C_4H_8 profiles closely overlap each other but not the H_2O profile.

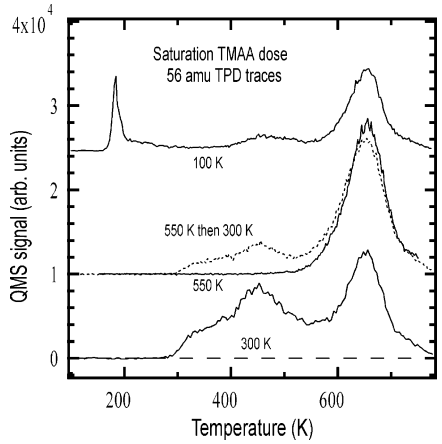

Figure 7. 56 amu TPD profiles for TMAA dosed with TiO_2(110) held at the indicated temperatures. In each case, the dose was sufficient to saturate the intensity above 300 K. The curve labeled "550 K then 300 K" denotes an experiment involving saturation at 550 K followed by cooling and saturation at 300 K before TPD.

geometries. The size, as determined from measured liquid-phase densities, implies, for these three species, that saturation monolayer coverage corresponds to an adsorbate/Ti^{4+} ratio no greater than 0.7. Since directly dosed monolayer isobutane desorption is, at best, weakly chemisorbed and, for multilayer doses, distinguishable only as a shoulder on the multilayer peak, we used the value of $0.7 \times (5.2 \times 10^{14})$ cm^{-2}. An isobutene monolayer is chemisorbed, likely involving interaction of the electron density in its π bonds as a means of shifting the coordination number of exposed Ti^{4+} from 5 toward the fully coordinated value of 6. In this geometry, the C═C bond lies parallel to and along the Ti^{4+} rows at the surface and the predicted saturation adsorbate/Ti^{4+} ratio is 0.5. Similar considerations apply to TMAA; the two carboxylate oxygens provide electron density to fill the coordination shells of pairs of exposed Ti^{4+}, i.e., at saturation, the adsorbate/Ti^{4+} ratio is, again, 0.5. Supporting this, the saturation ratio for deprotonated TMAA, i.e., TMA/Ti^{4+}, directly determined by AFM/STM, is 0.5.[2,4]

Returning to a discussion of Figure 5, the following qualitative picture emerges for TMAA dosed at 100 K. For $D < 1.0$, all the TMAA deprotonates, i.e., none desorbs below 300 K. For $D < 0.25$, very little of the TMA reprotonates. Since the carbon monoxide and isobutene intensities grow linearly with dose, it is intuitively reasonable to suppose that in the early stages, the absence of TMAA desorption is compensated by relatively larger amounts of (isobutane + MIK) and water.

Each normalized to maximum intensity, comparing the background-subtracted water, carbon monoxide, and isobutene profiles is revealing, Figure 6. Above 300 K, H_2O desorption peaks at 480 and 680 K whereas CO and i-C_4H_8 exhibit strong peaks at 660 K with very little desorption between 300 and 550 K. The desorption of water (i.e., removal of H and O from the surface) at temperatures much lower than the desorption of CO and i-C_4H_8 must be accounted for in any acceptable mechanism. As we shall see, bridging oxygen atoms are incorporated in the H_2O and CO that desorbs. The high-temperature desorption of water, delayed with respect to CO and i-C_4H_8, accounts for ~35% of the total H_2O and can be accounted for, at least in part, by the process that leads to MIK desorption (see below). The baseline above 700 K is uncertain, underscoring the difficulty of determining the absolute amount of water desorbing in this system.

Following the procedure described above, Table 2 summarizes the absolute coverages calculated from the TPD profiles for saturation doses at 300 and 550 K, and Figure 7 shows saturation (above 300 K) 56 amu TPD profiles for doses at 100, 300, 550, and 550 followed by additional exposure at 300 K. From Figure 7 and as noted above, it is clear that, compared to 100 K, saturation at 300 K uniformly increases the 56 amu intensity profile above 300 K. After accounting for fragmentation and sensitivity, Table 2 indicates the amount of isobutene desorbing above 300 K is 3-fold larger. Compared to dosing at 300 and 100 K, saturation at 550 K gives significantly stronger intensity in the 660 K peak. The dashed curve of Figure 7 shows the 56 amu profile after a saturation dose at 550 K followed by a saturation dose at 300 K and underscores an important point: saturation at 550 K does not fill all available adsorption sites on TiO_2(110). We will return to this point when describing product desorption during dosing.

According to Table 2, compared to 100 K, saturation at 300 K more than doubles the summed amount of isobutene + TMAA + isobutene + MIK. Expressed as ML, where 1 ML is defined as the number of exposed Ti^{4+} on a perfect TiO_2(110) surface (5.2×10^{14} cm^{-2}), the sum increases from 0.22 to 0.58 ML. Saturation at 550 K gives 0.30 ML, while saturation at 550 followed by saturation at 300 K gives 0.45 ML. Given the uncertainties in the calculated amounts (10%), these sums clearly fall into two regimes—quarter and half monolayer. It is worth noting that the (isobutene + MIK)/(isobutene) ratio is 0.25 for all the dosing conditions. Water desorption, as above, is more uncertain, but interesting qualitative comparisons can be made. At 100 K, the amount of water desorbed is 88% of the sum

TABLE 2: Absolute Amounts Desorbed above 300 K for Various Dosing Temperatures

dose T/K	(isobutane + MIK)/ 10^{13} cm^{-2}	isobutene/ 10^{13} cm^{-2}	TMAA + di-*tert*-butyl ketone/10^{13} cm^{-2}	water/ 10^{13} cm^{-2}	ML total
100	1.15 (0.81)	4.24 (0.84)	6.06 (0.27)	4.76	0.22
300	3.21 (0.60)	12.0 (0.55)	15.3 (0.19)	15.7	0.58
550	2.11 (1.00)	8.31(1.00)	4.9(1.00)	4.12	0.30
550 then 300	2.73	10.4	10.4	7.07	0.45

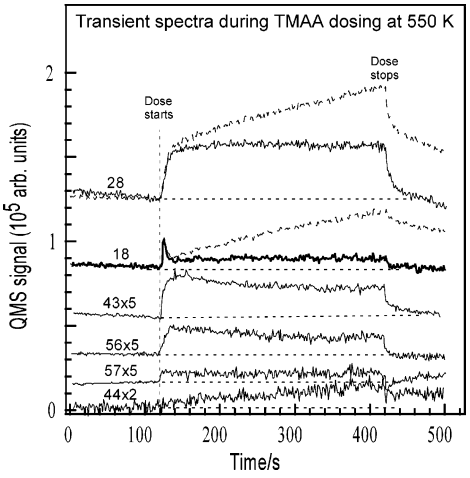

Figure 8. Isothermal reaction spectra of indicated ions when TiO_2-(110) held at 550 K was dosed with TMAA. The dose began at 120 s and terminated 300 s later at 420 s. For 28 and 18 amu, there are two curves. The steadily rising curve is the raw data and, as described in the text, the second curve has been adjusted to account for the steadily rising base pressure in the vacuum chamber during dosing.

(isobutene + isobutene + MIK), whereas it is 103% at 300 K. This ratio drops by more than a factor of 2 when the procedure involves dosing at 550 K. Keeping in mind that Table 2 only considers desorption above 300 K, there is one other interesting empirical observation. The amount of TMAA desorbed, for 100 and 300 but not 550 K doses, is approximately equal to the sum isobutene + isobutene + MIK.

From the TPD spectra of Figure 1, desorption above 300 K has peaks in two broad regions—300 to 550 K and 550 to 750 K. In parentheses, Table 2 provides the fraction of each component of that appears above 550 K for doses at 100, 300, and 550 K, e.g., the fractions are all unity for saturation doses at 550 K.

Desorption during Dosing. Monitoring products desorbing during dosing is helpful. After making background corrections, Figure 8 shows as solid curves, intensity profiles before, during, and after TMAA dosing at 550 K. Following a 120 s background gathering period, dosing commenced. After 300 s, dosing stopped and signals were followed toward background levels. Before the dose started, the I_{43}, I_{56}, and I_{57} signals were negligible, while I_{18}, I_{28}, and I_{44} were relatively intense. With one exception, 44 amu, all the uncorrected, i.e., measured, signals exhibit sharp onsets followed by a nearly linear rise to the end of the dose where the signals decay exponentially. I_{44} rises linearly with dose time without a sharp onset. Two examples of measured profiles, I_{28} and I_{18}, are shown in Figure 8 (dashed lines). The linear rises are attributed to the background response of the system to the dosing of TMAA. For comparison, we placed a stainless steel flag between the substrate and the doser and recorded profiles for the same masses. This set of profiles was used to remove backgound from the measured signals giving the solid curves of Figure 8. Pairs of profiles were subtracted and the difference was then adjusted by small linear background to account for the 10% higher response of the system when dosing on the sample, as reflected in the rising difference curve for I_{44} (curve at bottom of Figure 8). Since dosing the flag accounts for much of the nonreactive scattering of TMAA, the constant intensities beyond the onset transients indicate that a condition is reached where, at constant rates, TMAA, *i*-C_4H_{10}, MIK, *i*-C_4H_8, di-*t*-BK, CO, and H_2O form and desorb.

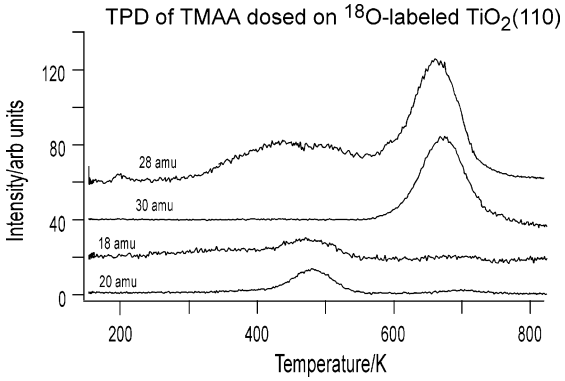

Figure 9. TPD after dosing TMAA onto TiO_2(110) labeled with ^{18}O. The 20 amu profile is diagnostic for $H_2{}^{18}O$ and the 30 amu for $C^{18}O$.

The onset characteristics of these signals differ. While I_{28} and I_{57} rise promptly to constant values, I_{18} has a sharp peak, I_{43} is characterized by an increasing rate for the first 40 s and then appears to drop slightly before reaching steady-state, and I_{56} reaches a maximum quickly but then drops slightly before becoming, as all other signals, nearly constant beyond 300 s. The absence of a sharp onset for I_{44} indicates negligible reaction on the substrate to form CO_2.

For the analogous experiment at 300 K, there are only two detectable differences between dosing the flag and dosing the substrate. First, as expected, the signals from dosing the sample are 1.1- to 1.2-fold larger than those for dosing the flag. Second, only for 57 amu, are there nonnegligible differences between the scaled signal for dosing the flag and the unscaled signal for dosing the substrate. Scaling the 57 signal from the flag by the minimum value, 1.1, leads to a difference signal for the first 2 min of dosing. The integrated difference rises monotonically from 120 s (the dosing onset) to 240 s where it drops to zero and the integral becomes constant, indicating that the substrate is saturated (not shown). The constant value beyond 240 s can be taken as a measure of the maximum dissociative adsorption (deprotonation) of TMAA on TiO_2(110) at 300 K. The absence of detectable differences at all the other masses indicates that TMAA adsorption at 300 K does not lead to transient or steady-state gas-phase product formation.

Oxygen Isotope Labeling. In one set of experiments, the TiO_2(110) surface and subsurface were labeled with ^{18}O by dosing with $^{18}O_2$.[11] Figure 9 shows how this influences the resulting intensity profiles for masses 18, 20, 28, and 30. Comparing I_{18} ($H_2{}^{16}O^+$) and I_{20} ($H_2{}^{18}O^+$) clearly exhibits extensive incorporation of oxygen atoms initially in the lattice into the desorbing water. At each temperature from 400 to 800 K, roughly 50% of the oxygen is from the lattice. The 28 ($C^{16}O^+$) and 30 ($C^{18}O^+$) amu profiles are distinctly different. For $C^{18}O$, there is no intensity above background below 550 K but intensity roughly equal to $C^{16}O$ above 550 K. While fragmentation adjustments lead to some uncertainty in the 28 amu signal attributable to CO desorption, it is clear that lattice oxygen becomes incorporated in desorbing CO only above 550 K. It is worth noting that the amu 28 and 30 peaks do not have the same peak temperature; the latter peaks at a slightly higher temperature. This suggests that decomposition without scrambling has a slightly faster rate than decomposition with scrambling.[3]

X-ray Photoelectron Spectroscopy. To probe the chemical composition of the adsorbed species, XPS data was taken for the O(1s), C(1s), and Ti(2p) regions before and after TMAA was dosed to saturation at 300 K, annealed to selected temperatures, and recooled to 300 K. The C(1s) spectra (Figure

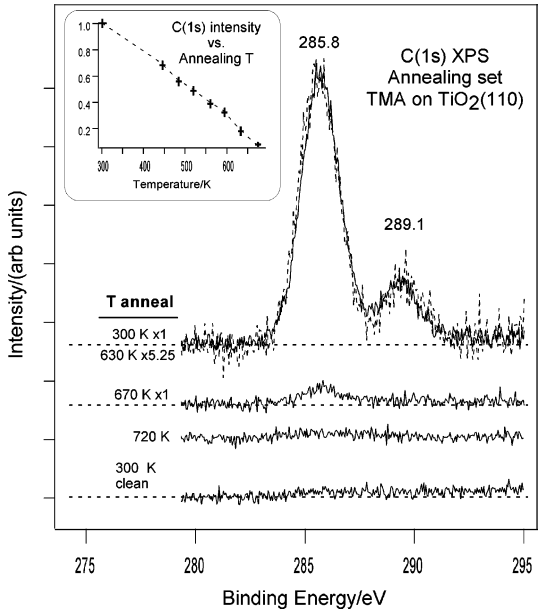

Figure 10. The C(1s) XPS region for TMAA dosed to saturation at 300 K, annealed to the indicated temperature, and cooled to 300 K for XPS. The inset shows the integrated C(1s) signal as a function of annealing temperature. The 300 K curve and the 630 K profile, after scaling by 5.25×, exhibit excellent overlap.

10) obviously comprise two components. Consider first the spectrum for the as-dosed overlayer. Assuming a symmetric line shape for each component determined by the leading edge of the low BE (LBE) component and the trailing edge of the high BE (HBE) component, we empirically constructed model contributions by combining the HBE trailing edge with its mirror image and the LBE leading edge with its mirror image. The resulting constructions when superimposed, faithfully overlap the full spectrum. When the HBE component is scaled by 4.5×, there is excellent overlap with the LBE component (not shown). We conclude that this two-component decomposition with peaks at 285.8 and 289.1 eV BE reliably describes the data. The higher BE peak is associated with the carboxylate carbon and the lower BE peak with the carbon atoms comprising the *tert*-butyl group.

The intensity ratio, $I_{LBE}/I_{HBE} = 4.5 \pm 0.2$, is measurably higher than the ratio of 4.0 in TMA. This is consistent with expectations, namely, TMA oriented with the *tert*-butyl group pointed away from surface. As a result, the HBE C(1s) signal is attenuated slightly by scattering as electrons pass through the *tert*-butyl groups.

Annealing the TMA-saturated surface to selected temperatures up to 625 K (followed by cooling to 300 K for XPS), gave C(1s) spectra with monotonically declining intensity (inset) but no distinguishable change in peak position, relative intensity or line shape between 300 and 630 K. As shown in Figure 10, the spectrum taken after heating to 625 K, when multiplied by 5.5, exhibits excellent overlap with that taken after the 300 K dose. While there is clearly a detectable HBE C(1s) signal after annealing to 670 K, the signal-to-noise ratio precludes determining the I_{LBE}/I_{HBE} ratio. Reflecting full removal of C-containing species, there is no detectable C(1s) signal after annealing to 720 K. The XPS and TPD results agree in the sense that heating from 300 to 550 K reduces the C(1s) intensity to 0.4 of its initial value within experimental uncertainty of that estimated (0.44) from the analysis of the TPD products (Table 2).

Turning to O(1s) spectra, Figure 11, comparing clean and TMA-saturated TiO_2(110), reveals differences reflecting the presence of chemically distinct adsorbate and substrate oxygen

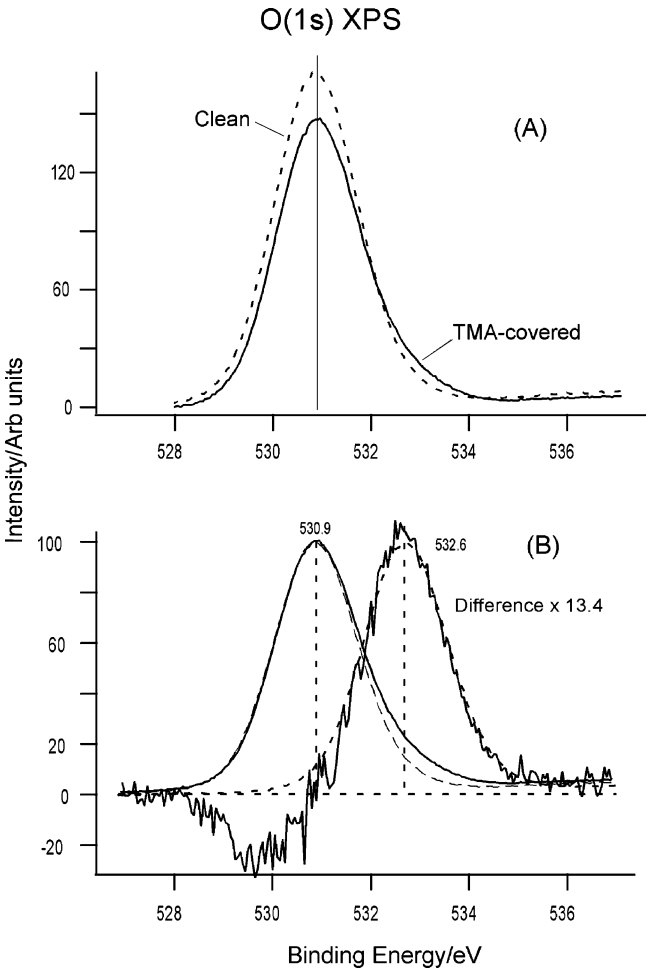

Figure 11. Panel (A) is the O(1s) XPS region for clean and TMA-saturated TiO_2(110). The maximum is located at 530.9 eV. Panel (B) shows (left side) the curves of panel (A) normalized to 100 units at their maxima and (right side) the difference (TMA-covered minus clean) scaled by 13.4× (noisy curve) and laid over a shifted replica of the clean surface curve.

atoms. While both sets of raw data, panel (A), show a single peak at 530.9 (±0.1) eV BE, the maximum is less intense (0.89), the width larger, and the shape skewed toward higher BE for the adsorbate-saturated surface. These results reflect a single O(1s) environment on the clean surface that is attenuated when TMA is added. The O atoms of TMA are evident as high BE component that broadens the O(1s) profile. Normalizing the two raw spectra at their maxima and taking the difference gives a peak at 532.6 (±0.3) eV. Figure 11 shows that this peak when scaled by 13.4× overlaps a shifted reproduction of the clean surface signal (panel B).

The Ti(2p) spectra of clean and TMA-saturated TiO_2(110) are also informative (Figure 12) and consistent with the conclusions drawn from the C(1s) and O(1s) spectra. The two raw spectra have identical peak positions (459.6 and 465.2 ± 0.1 eV) with the expected spin−orbit splitting of 5.6 eV. Of greater significance, the signal from the TMA-covered surface is attenuated by an amount (0.84) comparable to that found (0.89) for the substrate portion of the O(1s) signal and the scaled version overlaps faithfully that of the TMA-covered surface as indicated by the difference spectrum, (A) − (B). Spectrum (C) is the difference between the initial clean surface and the carbon-free surface found after annealing the TMA-saturated surface to 720 K or higher (not shown). These results indicate that adding TMA simply attenuates the Ti(2p) signal without altering,

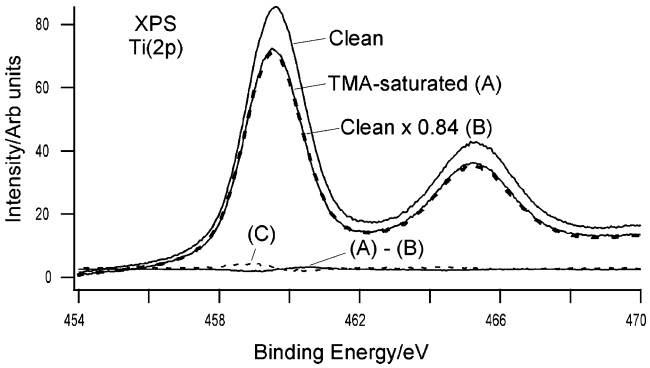

Figure 12. The Ti(2p) XPS region for clean and TMA-saturated TiO_2-(110), labeled (A), and for a scaled (0.84×) replica of the clean surface profile, labeled (B). The difference, (A) − (B), indicates negligible change brought about by dosing TMAA to saturation at 300 K. Curve (C) is the difference between the Ti(2p) profile taken of the clean surface and after annealing a TMA-saturated surface to 750 K. See Figure 8 for corresponding C(1s) profile.

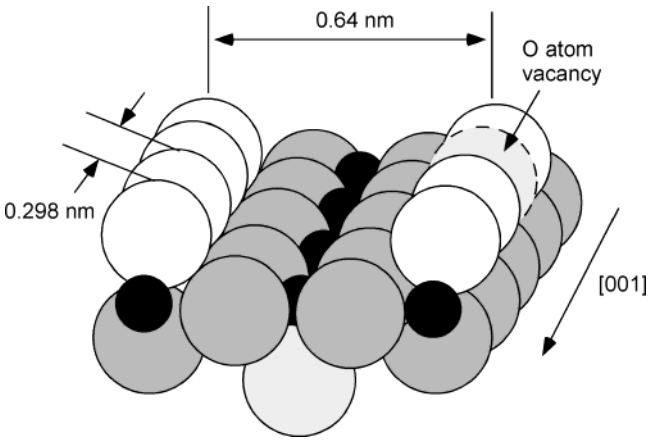

Figure 13. Schematic of a TiO_2(110) surface showing Ti^{4+} as small filled circles, bridging oxygen anions as open circles, and fully coordinated O^{2-} as filled gray circles. A bridging oxygen vacancy is depicted as the dashed curve. For our conditions, there approximately 1 vacancy for 15 bridging oxygen atoms. The [001] direction is parallel to the rows.

in a measurable way, the oxidation state of the Ti cations. Furthermore, even though lattice oxygen atoms are removed from the substrate in the desorbing H_2O and CO, the intensity ratio and the O(1s) and Ti(2p) line shapes obtained before dosing TMAA and after thermal desorption of TMA are indistinguishable.

IV. Discussion

We begin the discussion by reviewing the structures of the adsorbate and substrate. The structure of the surface of TiO_2-(110) is depicted in Figure 13.[1] It is characterized by rows of 5-coordinate Ti^{4+} cations that are separated by 0.298 nm along the [001] direction. The rows are separated 0.64 nm along the orthogonal direction. The absolute areal density of Ti^{4+} is 5.2×10^{14} cm^{-2}, and we define this as one monolayer (ML). An equal number of O^{2-} anions are arranged in parallel rows lying between the Ti^{4+} rows. These anions bridge pairs of Ti^{4+} lying beneath them. Annealing TiO_2(110) in a vacuum at elevated temperatures removes some oxygen-forming vacancies on the surface. In this process, a pair of Ti cations, formerly bridged by an oxygen atom, becomes exposed at the solid-vacuum interface. Each member of the pair is formally reduced to Ti^{3+} by acquiring an electron from the departing O^{2-}. For our crystal and vacuum annealing conditions (850 K for 10 min), there are 0.065 ± 0.010 ML of oxygen atom vacancies.

Trimethyl acetic acid has a single acid hydrogen and, like other organic acids, it deprotonates on the TiO_2 surface at 300 K by interacting with neighboring acidic (Ti^{4+}) and basic (O^{2-}) sites. Since, in the resulting carboxylate anion, there are two basic oxygen centers, a bidentate carboxylate with the carboxyl oxygen atoms bonded to neighboring Ti^{4+} centers is likely and is consistent with our data. The proton will bond to a bridging oxygen atom. The resulting carboxylate structure viewed from the side and from the top is depicted in Figure 14. In these views, it is important to note that the diameter of the *tert*-butyl group matches the dimensions of the titania lattice so that when viewed from the top, an ordered (2×1) overlayer, confirmed by STM images,[4] leaves no accessible acidic Ti^{4+} sites and severely limits access to the bridging O^{2-} sites, half of which are protonated.

Keeping these structures in mind, we discuss the thermal properties of the TMAA−TiO_2(110) system. When TMAA is exposed to TiO_2(110) at 100, 300, or 550 K, the same products appear in TPD but with differing distributions of relative and absolute intensities. Monitoring desorption during dosing reveals a steady-state gas−surface reaction when the substrate is held at 550 K. Scattering of TMAA, but no other species, occurs as the surface saturates when dosed at 300 K. When dosed at 100 K, no scattered species are detected. We conclude that TMAA dosed at 100 K adsorbs with near-unity sticking coefficient regardless of the dose, does not saturate, and adsorbs with little, if any, surface reaction. By comparison, TMAA dosed at 300 K adsorbs to saturation, i.e., does not form a multilayer, and the products formed by surface reactions are all retained at the surface.

In more detail for 100 K doses, the TPD intensities increase to saturation except for an unsaturable peak at 190 K that is attributed to multilayer desorption. The 100 K dose required to saturate the intensities above 300 K is defined as a unit dose ($D = 1$). The shoulder on the 190 K peak (Figure 1), attributed to TMAA in contact with TiO_2(110), saturates (not shown) for a larger dose ($\sim 2D$). The TPD for $D = 2$ also has much more intensity in the multilayer peak. We conclude that the as-dosed TMAA is disordered and, for D between 1 and 2, includes some multilayer islands. In TPD, some of the TMAA in these islands desorbs with multilayer characteristics while the remainder rearranges leaving a single layer of TMAA at 200 K. Between 200 and 250 K, the weakly chemisorbed TMAA either desorbs or, consistent with the deprotonation expected for 300 K doses,[2,9] deprotonates to form the carboxylate, $(CH_3)_3CCOO^-$, and hydroxide, OH^-, moieties depicted in Figure 14. Regardless of the coverage, these chemisorbed species are stable to at least 300 K. When D is less than 1, the TPD product distribution shows negligible desorption below 300 K, indicating that all the TMAA deprotonates.

For saturation doses, the products desorbed between 300 and 550 K for doses at either 100 or 300 K are dominated by TMAA and H_2O. For $D < 0.5$, H_2O is the only product with significant intensity in this region but as D increases from 0.5 to 1.0, more and more TMAA appears in this temperature interval. For all three dosing temperatures, the TPD products appearing above 550 K are dominated by *i*-C_4H_8, CO, and H_2O accompanied by smaller amounts of *i*-C_4H_{10}, MIK, and either or both TMAA and di-*t*-BK.

The stoichiometric reaction, $(CH_3)_3CCOO^- + H^+ \rightarrow$ *i*-C_4H_8 + CO + H_2O, accounts for the formation of isobutene, carbon monoxide, and water. While it cannot be an elementary step,

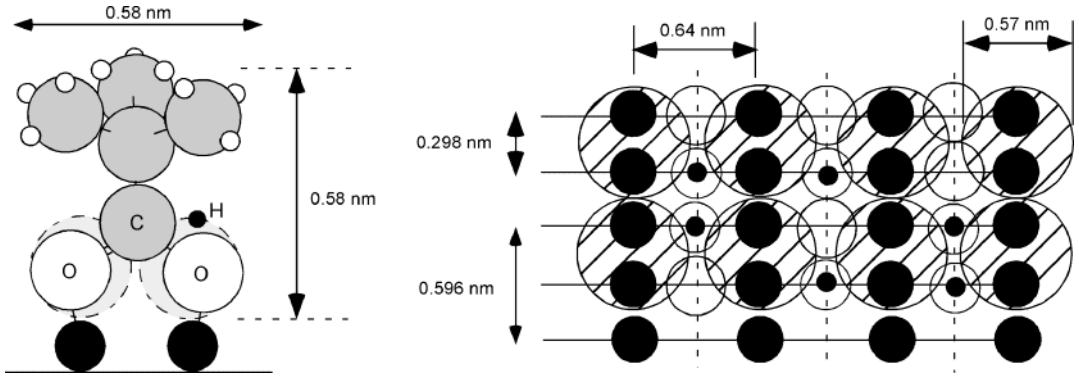

Figure 14. On $TiO_2(110)$, schematic depiction of bidentate trimethyl acetate bound to neighboring Ti^{4+} sites and proton bound to bridging oxygen atoms. Side view (left panel) and top view (right panel).

this overall reaction is an instructive starting point for further discussion (see below). Isobutane would be the result of hydrogenation of the *tert*-butyl group either on the TiO_2 surface or in a subsequent collision prior to ionization. The path to MIK involves concerted deprotonation of a methyl group and migration of a methyl group to the carbonyl carbon. This process can account for the high-temperature H_2O formation since OH^- will be the product of the deprotonation (see reaction 7 below).

Setting aside for now both the path to isobutane and desorption of multilayer coverages, the following reactions account for the desorbing $(CH_3)_3CCOOH$, *i*-C_4H_8, CO, MIK, di-*t*-BK, and H_2O. In the following, the italicized subscripts (g), (*a*) and (l) denote gas, adsorbed and lattice, respectively, and V denotes vacancy.

$$(CH_3)_3CCOOH_{(g)} \rightarrow (CH_3)_3CCOOH_{(a)} \quad (1)$$

$$(CH_3)_3CCOOH_{(a)} \rightarrow (CH_3)_3CCOOH_{(g)} \quad (2)$$

$$(CH_3)_3CCOOH_{(a)} + O^{2-}{}_{(l)} \rightarrow (CH_3)_3CCOO^-{}_{(a)} + O_{(l)}H^- \quad (3)$$

$$(CH_3)_3CCOO^-{}_{(a)} + O_{(l)}H^- \rightarrow (CH_3)_3CCOOH_{(g)} + O^{2-}{}_{(l)} \quad (4)$$

$$2O_{(l)}H^- \rightarrow H_2O_{(g)} + O^{2-}{}_{(l)} + V \quad (5)$$

$$(CH_3)_3CCOO^-{}_{(a)} + V \rightarrow CO_{(g)} + O_{(l)}H^- + i\text{-}C_4H_{8(g)} \quad (6)$$

$$(CH_3)_3CCOO^-{}_{(a)} + O^{2-}{}_{(l)} \rightarrow CH_2{=}C(CH_3)C(=O)CH_{3(g)} + O_{(l)}H^- \quad (7)$$

$$2(CH_3)_3CCOO^-{}_{(a)} + 2V \rightarrow (CH_3)_3CC(=O)C(CH_3)_{3(g)} + CO(g) + O^{2-}{}_{(l)} \quad (8)$$

During dosing at 100 K, reaction 1 is sufficient and, in subsequent TPD, reactions 2−8 all contribute. During dosing at 300 K, reactions 1−3 all contribute, and the accumulated surface concentration of $(CH_3)_3CCOOH_{(a)}$ is negligible. During subsequent TPD, reactions 4−8 contribute, but not reactions 1−3. During dosing at 550 K, all six reactions contribute to achieve the observed steady-state reaction and, during subsequent TPD, reactions 4−8 contribute with reactions 5 and 6 dominating.

Compared to a 100 K dose that saturates the intensity desorbed above 300 K, a saturation dose at 300 K leads to significantly higher intensity (Figure 7). We conclude that TMAA dosed at 100 K and in contact with $TiO_2(110)$ does not all deprotonate either at 100 K or during subsequent TPD; rather, much of the first layer desorbs between 200 and 250 K without intervening deprotonation.

During dosing at 300 K, incident TMAA molecules either react or scatter. Since TMAA is the only scattered species detected, the surface reactions must retain all the reaction products. The C(1s) core level photoemission data are consistent with deprotonation to trimethyl acetate, $(CH_3)_3CCOO^-$, with one or both of the oxygen atoms bound to Ti^{4+} and the *tert*-butyl group directed away from and not interacting with the titania surface. Saturation at 300 K is 0.58 ML, Table 2, and the surface is extremely hydrophobic.[5] Within experimental uncertainty, this coverage equals that (0.5 ML) independently measured by STM,[4] the latter showing the carboxylate species form an ordered (2×1) overlayer aligned along the Ti^{4+} rows and centered over them, Figure 14.

For doses at 100 and 300 K, the TPD and XPS data reflect steady loss of carbon as the temperature passes from 300 to 750 K. Between 300 and 550 K, this is largely the result of reprotonation of TMA to form and desorb TMAA (Table 2 and the values in parentheses). In parallel, some isobutene and isobutane or MIK desorbs.

Dosing at 550 K differs. During dosing, a steady-state reaction condition is realized that prevents filling of all available adsorption sites. TPD, after maximizing the coverage at 550 K, stopping the dose, and rapidly cooling, gives a coverage of 0.30 ML, half the saturation value achieved by dosing at 300 K, Table 2. As expected, there is no intensity below 550 K except for small amounts of background accumulation. The intense desorption peaking at 660 K, is dominated by isobutene and CO with some TMAA, MIK, di-*t*-BK, and *i*-C_4H_{10} (Table 2). During neither dosing nor subsequent TPD is there any evidence for CO_2 or H_2 desorption.

The steady-state reactivity realized during 550 K doses implies that the ensemble-average surface concentrations are not changing. This indicates that the number of surface sites involved in converting TMAA to products remains a constant fraction of 5.2×10^{14} cm^{-2}. On the basis of the coverage achieved at steady-state, half these sites are not occupied at any given instant. The steady-state nature of the reactivity also implies that the titania surface, unlike most transition metal surfaces, is not becoming cluttered with unreactive carbon-

containing fragments that inhibit reaction. This is consistent with the XPS and AES data showing a carbon-free surface after TPD to 750 K.

In TPD, water desorption makes an important contribution. For doses at 100 and 300 K, a large fraction (~65%) of the water desorption occurs before most of the CO desorbs. This water peaks at 480 K, near the desorption peak temperature (500 K) found for recombination of OH groups formed from H_2O dosed on a TiO_2(110) surface containing oxygen atom vacancies.[6] Evidently, the presence of TMA moieties does not alter, in any major way, the disproportionation of hydroxide groups to form water. Consistent with the incorporation of lattice oxygen atoms evidenced by ^{18}O labeling, we conclude that the 480 K water desorption creates, but only transiently, a large number of oxygen atom vacancies. Significantly, for all dosing temperatures there is a peak that trails the maximum rate of isobutene and CO desorption (660 K). For doses at 100 K, roughly 35% of the water desorption occurs in this high-temperature peak. This water is always observed when TMAA is dosed and is always absent when water, itself, is dosed. We propose that the reaction path leading to it is related to the process of MIK formation, reaction 7 above. It is noteworthy that the intensity in this peak grows with the intensity of water at 480 K and with the intensities of species peaking at 660 K, i.e., the fraction remains near 35% for all 100 and 300 K doses. This points to a precursor related to the amount of TMA that survives to 550 K.

Recalling that, even though lattice oxygen atoms are removed, XPS indicates no change in either the TiO_2(110) surface stoichiometry or the Ti oxidation state when TMAA is adsorbed at 300 K and the resulting TMA is heated to 750 K. We conclude that the lattice oxygen atoms that are incorporated in the desorbed H_2O and CO are replaced by oxygen from the dosed TMAA. Apparently, reaction of activated TMA above 550 K fills the vacancy by a sequence of coupled steps. The overall process likely involves exchanging oxygen isotopes between the lattice and TMA, rearranging TMA into either CO and isobutene or MIK, and partitioning the excess O and H into the previously formed vacancies and H_2O. These processes can account for the high-temperature water desorption signal.

In this context, the sharp transient peak in the water profile when dosing at 550 K is interesting. When dosing starts, deprotonation is rapid and the temperature is high enough to form and desorb water by disproportionation of hydroxides located along bridging oxygen atom rows. Rapid proton migration along the rows brings these hydroxides together for reaction. The initially rapid water formation rate is determined by the zero-coverage TMAA adsorption rate. The steady-state rate of water formation is reduced because, statistically, half the sites from which deprotonation occur are always filled.

The stoichiometric relations among the desorbed amounts shown in Tables 1 and 2 depend on the reaction path taken by dosed TMAA. These considerations are constrained by two important facts: (1) regardless of the dosing temperature, the surface is carbon-free after TPD to 750 K, and (2) only TMAA, isobutene, water, carbon monoxide, di-*t*-BK, and either or both MIK and isobutane desorb in significant amounts. For doses at 100 K and focusing on saturation (Table 1), we assume every TMAA, isobutene, MIK, di-*t*-BK, and isobutane molecule that desorbs above 300 K is traceable to adsorbed TMA. Then saturation at 100 K involves 1.15×10^{14} TMAA cm^{-2} (0.44 ML) that are not involved in desorption below 300 K. Assuming, sensibly, that one CO desorbs for every TMA that is lost, the predicted CO intensity is 5.39×10^{13} cm^{-2}, a value 90% of that calculated. Given the uncertainties involved, better agreement is not expected. We now consider the water desorption. Each dosed TMAA delivers 10 H atoms to the surface. Since there is no detectable H_2 desorption, these 10 atoms must be desorbed in other H-containing molecules, i.e., H_2O, *i*-C_4H_8, *i*-C_4H_{10}, MIK, di-*t*-BK, and TMAA. This immediately leads to the conclusion that, on the basis of the H atoms, the H_2O/*i*-C_4H_8 ratio should lie near unity, whereas the ratio calculated from Table 1 is 12% higher (1.12), but within expected uncertainty limits, particularly for the amount of water desorbed and the uncertainties in assigning product distributions at the 660 K peak.

On the basis of independent STM[4] evidence that saturation at 300 K forms an ordered (2×1) overlayer of trimethyl acetate with one acetate for each pair of Ti^{4+} at the surface of TiO_2-(110), monolayer coverage is 2.6×10^{14} carboxylates cm^{-2}. According to the above interpretation, 50% (1.3×10^{14} cm^{-2}) of these desorb as TMAA, 45% as isobutene, and 5% as isobutene + MIK. For a 550 K dose, the subsequent TPD indicates half as many carboxylates (1.3×10^{14} cm^{-2}) and, of these, 59% desorb as isobutene, 31% as TMAA + di-*t*-BK, and 10% as isobutene + MIK.

Among the organic acids that have been studied,[2] TMAA is relatively unique in at least two respects—a tertiary carbon atom is bound to the carboxyl carbon and the size is closely matched to the TiO_2(110) unit cell. The tertiary nature of the β-carbon in the R group of the carboxylate precludes β-carbon dehydrogenation, a reaction typical of primary and secondary organic carbons. Removing this channel increases the thermal stability of trimethyl acetate. Compared to formate,[3] for example, the decomposition temperature of trimethyl acetate, is about 100 K higher.

An important property of TiO_2(110), and other reducible transition metal oxides, is the facile turnover of surface oxygen atoms. In catalytic processes, atoms from such catalysts appear in the products and are replaced by chemically identical atoms from the reactants. For TiO_2, the bridging oxygens are incorporated in desorbing products, for example, isotope labeling of a TiO_2 surface with ^{18}O followed by dosing unlabeled formic acid leads to ^{18}O-labeled water.[3] SIMS results indicate that exchange of ^{18}O from lattice into C-containing species derived from formate sets in when CO begins to desorb (~400 K) and grows rapidly between 400 and 550 K.

V. Conclusions

Trimethyl acetic acid dosed onto a clean and systematically annealed TiO_2(110) surface deprotonates to form trimethyl acetate and hydroxide groups that, for small submonolayer coverages, react during thermal desorption to form and desorb large amounts of carbon monoxide and isobutene and smaller amounts of methyl isopropenyl ketone, di-*tert*-butyl ketone, and isobutane, all peaking at 660 K, and water peaking at 480 and 680 K. As the dose increases, reprotonation to reform and desorb trimethyl acetic acid plays an increasing role. Calibrated desorbing intensities indicate that saturation at 300 K lies near half monolayer of trimethyl acetate ($\sim 2.6 \times 10^{14}$ cm^{-2}) in agreement with independently reported STM measurements. Maximum coverage at 550 K, on the other hand, is only quarter monolayer because a steady-state reaction occurs to continually remove adsorbed species without accumulating inhibitory carbon-containing species.

Acknowledgment. This work was supported by the U.S. Department of Energy, Office of Basic Energy Sciences, Division of Chemical Sciences. Pacific Northwest National

Laboratory is a multiprogram national laboratory operated for the U.S. Department of Energy by the Battelle Memorial Institute under Contract DE-AC06-76RLO 1830. The research reported here was performed in the William R. Wiley Environmental Molecular Science Laboratory, a Department of Energy user facility funded by the Office of Biological and Environmental Research. J.M.W. acknowledges support by the U.S. Department of Energy, Office of Basic Energy Sciences, Division of Chemical Sciences, the Center for Materials Chemistry at the University of Texas at Austin and the Robert A. Welch Foundation.

References and Notes

(1) Diebold, U. *Surf. Sci. Rep*. **2003,** *48*, 53. A review of the surface science of titanium dioxide with numerous references cited.

(2) Sasahara, A.; Uetsuka, H.; Onishi, H. *Surf. Sci*. **2001,** *481* L437; Onishi, H. Springer Series in Chemical Physics **2003**, *70* (Chemistry of Nanomolecular Systems), 75.

(3) Henderson, M. A. *J. Phys. Chem*. B **1997**, *101*, 221.

(4) Henderson, M. A.; White, J. M.; Uetsuka, H.; Onishi, H. *J. Am. Chem. Soc*. **2003**, *125*, 14974.

(5) White, J. M.; Szanyi, J.; Henderson, M. A. *J. Phys. Chem*. B **2003**, *107*, 9029.

(6) Henderson, M. A. *Surf. Sci. Rep*. **2002,** *46*, 1; Henderson, M. A. *Surf. Sci*. **1994**, *319*, 315; Henderson, M. A. *Langmuir* **1996**, *12*, 5093.

(7) NIST Chemistry WebBook, http://webbook.nist.gov/chemistry/.

(8) Onishi, H. Private communication.

(9) White, J. M.; Henderson, M. A. To be published.

(10) Linsebigler, A.; Lu, G.; Yates, J. T., Jr. *J. Chem. Phys*. **1995,** *103*, 9438.

(11) Li, M.; Hebenstreit, W.; Gross, L.; Diebold, U.; Henderson, M. A.; Jennison, D. R.; Schultz, P. A.; Sears, M. P. *Surf. Sci*. **1999**, *437*, 173.